RESEARCH ARTICLE

Gambogenic Acid Enhances Oxidative Stress and Apoptosis by Suppressing Canine Osteosarcoma Cell Growth Via Autophagy Overactivation

Siyao Li[1‡], Yuan Zhao[1‡], Xiaoyu Hou[1‡], Huijie Kang[1], Qingdian Hou[1], Tianyuan Yang[1], Yuntong Zhang[1], Shuai Zhang[1], Weiqian Wang[1], Meimei Wang[1], Guangmin Zhang[1], Junping Sun[1], Jichen Sha[1*] and Honggang Fan[1*]

[1]Heilongjiang Key Laboratory for Laboratory Animals and Comparative Medicine, College of Veterinary Medicine, Northeast Agricultural University, Harbin, 150030, China. ‡ Siyao Li, Yuan Zhao, and Xiaoyu Hou contributed equally to this work.
*Corresponding author: sjc04291@163.com; fanhonggang2002@163.com

A B S T R A C T

Canine osteosarcoma is a highly aggressive bone malignancy characterized by rapid progression and a propensity for early metastasis. Gambogenic acid (GNA), derived from *Fructus garcinia*, possesses a broad spectrum of bioactive effects, including anticancer, antimicrobial, antiviral, anti-inflammatory, and antioxidant properties. In this research, the canine osteosarcoma cell line McKinley was chosen to investigate the mechanisms of GNA through autophagy, thereby offering a theoretical foundation for GNA in the treatment of canine osteosarcoma. Various concentrations of GNA were utilized to assess malignant biological characteristics, including proliferation, migration, and invasion in McKinley. Furthermore, we measured the levels of oxidative stress, mitochondrial dynamics, autophagy-related indicators, and apoptosis-related indicators. The results showed that GNA demonstrated an inhibitory effect on McKinley cells, with an IC_{50} value of 0.28μM, confirming a dose-dependent reduction in cell proliferation, migration, and invasion. McKinley cells exhibited increased oxidative stress levels, reduced mitochondrial membrane potential, and impaired mitochondrial functionality. Moreover, there was a substantial increase in the number of autophagosomes and elevated expression levels of autophagy-related protein and mRNA, and autophagy flow proceeded smoothly. Additionally, the apoptosis rate increased, accompanied by elevated levels of the pro-apoptotic proteins. Notably, 3-Methyladenine was found to counteract the inhibitory effects of GNA on the proliferation, invasion, and migration of McKinley cells, as well as to alleviate the oxidative stress and apoptotic effects induced by GNA. In conclusion, this study demonstrated the mechanism of action of GNA in the treatment of canine osteosarcoma.

To Cite This Article: Li S, Zhao Y, Hou X, Kang H, Hou Q, Yang T, Zhang Y, Zhang S, Wang W, Wang M, Zhang G, Sun J, Sha J and Fan H 2025. Gambogenic acid enhances oxidative stress and apoptosis by suppressing canine osteosarcoma cell growth via autophagy overactivation. Pak Vet J. http://dx.doi.org/10.29261/pakvetj/2025.238

INTRODUCTION

Canine osteosarcoma (OS) is an extremely malignant, rapidly progressive, and metastatic condition, representing 85% of all bone tumor cases in dogs (Poon *et al*., 2020). Medium and large dogs typically used to employ in various roles such as police, guide, and herding dogs in practical applications exhibit a heightened susceptibility to OS. This presents a considerable risk to the health and welfare of working dogs. Similar to humans, both the youth and the elderly stages are at risk of suffering from this condition. Dogs share comparable genes, epidemiology, and pathogenesis with humans, which leads to analogous drug

responses (Weiss *et al*., 2022). Numerous clinical drug trials rely on canine tumor models, particularly for rare instances of OS. Establishing safe and effective treatments can alleviate the pain associated with the disease and enhance animal welfare; furthermore, research on treating canine OS provides more valuable insights for humans. Currently, the standard treatment protocol for OS involves adjuvant chemotherapy with platinum-based antineoplastic drugs such as cisplatin and carboplatin after amputation (Selmic *et al*., 2014). However, the median survival remains short due to the presence of micro-metastases in the lungs in 90% of cases (Poon *et al*., 2020), compounded by the variable sensitivity to chemotherapy and the

significant side effects associated with chemotherapeutic drugs. Recent advancements in immunotherapies and targeted therapies have remained technically immature in recent years. Therefore, pursuing effective and safe drugs is essential for treating canine OS.

Tumor is the first disease identified to be associated with autophagy dysregulation, and the role of autophagy in cancer is complex and dualistic. Research indicates that before tumorigenesis, autophagy generally functions as a tumor suppressor, with selective autophagy targeting damaged mitochondria to mitigate ROS accumulation, which can adversely affect proteins, lipids, and DNA. However, in the advanced stage of cancer progression, autophagy becomes intricately associated with drug resistance, metastasis, and poor prognosis (Aqbi *et al.*, 2018; Fujii *et al.*, 2008; Wei *et al.*, 2014). Furthermore, autophagy plays a crucial role in the development of OS. The silencing of ARID3A has been shown to downregulate BECN1, thereby promoting the proliferation of U2OS cells (Parlayan *et al.*, 2021). Conversely, the overexpression of valosin-containing protein (VCP), a member of the ATPase superfamily, can activate the ERK/NF-κB/Beclin1 signaling pathway, thereby enhancing autophagy-mediated tumor anoikis and facilitating OS metastasis (Long *et al.*, 2019). Therefore, the role of autophagy in canine OS remains to be determined.

Gambogenic acid (GNA) is a naturally occurring compound derived from *Fructus garcinia* (Huang *et al.*, 2024). GNA is characterized by its stability in physicochemical properties, simplicity in the extraction process, and low cost. GNA demonstrates a range of biologically active effects, including anti-tumor, anti-inflammatory and anti-oxidant activities, which can significantly inhibit various tumors such as melanoma and multiple myeloma (Chen *et al.*, 2017; Wang *et al.*, 2022). Furthermore, GNA has extensive applications in regulating the oxidative stress and autophagy levels in diverse tumor cells, promoting apoptosis and thereby inhibiting tumor growth (Wang *et al.*, 2014; Wu *et al.*, 2023). Furthermore, GNA markedly inhibited tumor growth in the OS xenograft mouse model, leading to oxidative stress that triggers ferroptosis and apoptosis (Liu *et al.*, 2023). It is important to note that the precise function of autophagy in GNA's action against canine OS remains ambiguous.

In this research, McKinley cells were applied to examine the inhibitory impact of GNA, and to elucidate the mechanisms underlying its antitumor properties through autophagy. This study aims to lay a theoretical foundation for the practical application of GNA in canine OS, thereby enhancing its potential for tumor therapy, while also supporting theoretical insights for the treatment of OS within the realms of comparative medicine.

MATERIALS AND METHODS

Cell lines and cell culture: The canine OS cell line McKinley was provided by Colorado State University Flint Animal Cancer Center (FACC). The canine kidney cell line MDCK was purchased from Wuhan Procell Life Technology Co., Ltd (China). The cells were cultured in DMEM supplemented with 10% fetal bovine serum (China) at 37°C with 5% CO_2. GNA (USA) was dissolved in DMSO to create a reserve solution at 1mM. The working

solutions of GNA were prepared at concentrations of 0.32μM (GNA-H group), 0.28μM (GNA-M group), and 0.24μM (GNA-L group). These concentration gradients corresponded to 30%,50%, and 70% viability in McKinley cells (Huang *et al.*, 2018). Additionally, the working solution for the CQ group was 50μM Chloroquine (USA), and for the GNA-M+CQ group, it was 0.28μM GNA+50μM CQ. The working solution for the 3-MA group was 350μM 3-Methyladenine (USA), and for the GNA-M+3-MA group, it was 0.28μM GNA+350μM 3-MA. All working solutions were utilized to the cells for 48h.

Cell toxicity assays: McKinley cells in 96-well plates were treated with GNA and 3-MA for 48h. Cell viability was assessed using the Enhanced Cell Counting Kit-8 (China) by measuring absorbance at 450nm.

Cell wound healing assay: The McKinley cells were inserted into a 12-well plate. Subsequently, a 10μL pipette tip was used to establish the wound. GNA and 3-MA were used to treat cells. The images were captured at 0h, 4h, 8h, and 12h (Pan *et al.*, 2022).

Transwell assay: McKinley cells were inserted into the Transwell upper chambers for 48h. The upper chamber was fixed and stained with 0.1% crystal violet, and then images were taken. For invasion assay, Matrigel (China) was spread in the upper chamber (Pan *et al.*, 2022).

Detection of indicators related to oxidative stress in cells: Reactive oxygen species (ROS) assay Kit (E004-1-1), superoxide dismutase (SOD) assay kit (A001-3-1), malondialdehyde (MDA) assay kit (A003-1-1), glutathione peroxidase (GSH-PX) assay kit (A005-1-1), and catalase (CAT) assay kit (A007-1-1) were purchased from Njjcbio (China). The procedures were conducted according to the instructions provided in these kits.

Ultrastructural observation of the cells: The cells were pre-fixed with 2.5% glutaraldehyde. They were then post-fixed by osmium tetroxide, subjected to gradient dehydration and immersion, embedded and aggregated. Subsequently, they were sectioned into 50-60nm-sized pieces and stained before being observed under a transmission electron microscope (Hitachi, Japan) (Tavakolikazerooni *et al.*, 2025).

AO staining assay: Cells were diluted with 2μg/mL of the AO mixed within normal saline (Macklin, A6009) working solution. After washing the cells with PBS, 1mL of staining solution was added to each well of a 6-well plate and incubated for 30min at room temperature protected from light. Inverted fluorescence microscope (Ex/Em=488/530 nm) was used for nucleic acid observation, image capture and autolysosome observation (Ex/Em=530/640 nm).

Cellular immunofluorescence assay: The cells were fixed, and 0.5% Triton-X 100 permeated. After blocking with 5% goat serum, the cells were incubated with the primary antibody at 4°C overnight. Secondary antibodies were incubated and then counterstained with DAPI (5μg/mL) after washing. Image capture using an inverted fluorescence (Pan *et al.*, 2022).

Real-time PCR assay: Eastep® Super Total RNA Extraction kit (China) was used for total cellular RNA extraction and GoScript™ reverse transcription kit (China) was used for getting cDNA. RT-PCR was performed with 2×SYBR Green qPCR Master Mix (USA) on a Roche 480 System (Roche, Switzerland). The relative expression of each gene was calculated in the $2^{-\Delta\Delta CT}$ method. Primers for genes are listed in Table 1 (Zhao *et al*., 2022).

Table 1: Primers for real-time PCR

Gene	Accession Number	Primer Sequences (5'-3')
ATG5	XM_038684281.1	F: CAGACAACAACTGAACGACCT
		R: TTTCCCCATCTTCAGGAGCAA
ATG7	XM_038426910.1	F: TTGCCCACAGCATCATCTTCG
		R: TCCCATCCGACCGCCTTG
ATG12	XM_038681206.1	F: CCCGAACCATTCAAGGACTCA
		R: CCATCACTGCCAAAACACTCA
BECN1	XM_038676393.1	F: CAGCATGGCCTTCCCTT
		R: CACCGTCAGATGCCTCCC
BAX	NM_001003011.1	F: GCCCTTTTGCTTCAGGGTTTC
		R: CCACTCGGAAGAAGACCTCAC
BCL2	NM_001002949.1	F: GCACCTGACGCCCTTCACC
		R: TCCCGGTTGACGCTCTCCACA
MAPILC3B	XM_038666837.1	F: CGTCGCACCTTCGAACAAAGA
		R: ATGCTGCTCTCGGATAAGTCG
CASP3	NM_001419299.1	F: ACAGCCCCTGGTTACTATTCCT
		R: TCAGCATCGCACAAAGTGAC
CASP9	NM_001031633.1	F: CCCCGAGTCAAGGCTCAC
		R: CCACCACGCAGCAGTCCA
PARP1	XM_038671656.1	F: ATCGTGAAGGGAACCAACTCC
		R: ACCGAAAGATCCAGTACCTGC
GAPDH	NM_001003142.2	F: TGCCTCCTGCACCACCAAC
		R: CCGTCACGCCACATCTTCCC

Western Blot Analysis: The proteins were separated and subsequently transferred onto PVDF membranes. Moreover, the PVDF membrane was blocked in 5% skim milk for 2h, followed by incubation with primary antibodies overnight at 4℃. Followed by incubation of secondary antibodies at room temperature for two hours, imaging was performed using the automated chemiluminescence imaging analysis system (Biotanon, China). Protein of grey value was analyzed using Image J (Zhao *et al*., 2022).

Statistical analysis: Data were expressed as mean±SD. Statistical analysis of data in this study was performed by the PASW Statistics 18 software (IL, USA). All data were normally distributed, and one-way analysis of variance between groups was performed. All graphs were drawn by GraphPad Prism 7 (San Diego, California).

RESULTS

GNA inhibited the proliferation, invasion, and migration of McKinley cells: The results of the CCK-8 assay are shown in Fig. 1A. The viability of McKinley cells exhibited a gradual decline with increasing doses of GNA, and the IC$_{50}$ for GNA at 48h was determined to be 0.28μM. The toxicity of GNA on MDCK cells was minimal, with a cell viability of 93.33% at the same concentration of 0.28μM. Observations of cell morphology revealed a gradual reduction in the rate of cell fusion in response to GNA treatment. Additionally, there was a notable presence of suspended cells and cellular debris observed along with a more compact and refractive cytoplasmic structure (Fig. 1B). Results from the clonogenic assay showed that the proliferation ability decreased in a dose-dependent manner under GNA (Fig. 1C). The migration capacity of cells treated with GNA was assessed through the cell wound healing assay (Fig. 1D), Transwell migration assay (Fig. 1E), and Transwell invasion assay (Fig. 1F). Compared to the CON group, a dose-dependent reduction in both migratory and invasive capabilities of GNA-treated cells was observed. Thus, it could be observed that GNA inhibited the proliferation, invasion, and migration of McKinley cells.

GNA enhanced oxidative stress, mitochondrial autophagy, and apoptosis in McKinley cells: The results of ROS levels in McKinley cells are illustrated in Fig. 2A. The ROS levels in the GNA group showed a significant increase as compared to the CON group. Consistent with this finding, the intracellular content of MDA also escalated with the dose of GNA, while the activities of SOD, GSH-PX, and CAT were significantly decreased (Fig. 2B). The mitochondrial membrane potential (MMP) was assessed by employing JC-10. In response to GNA, a significant reduction in the mitochondrial membrane potential of McKinley cells was observed (Fig. 2C). The expression levels of mitochondrial dynamics-related proteins are presented in Fig. 2D. Compared to the CON group, GNA significantly upregulated the expression of pro-mitochondrial fission proteins Drp1 and Mff, while downregulated the expression of pro-mitochondrial fusion proteins OPA1 and Mfn2. Furthermore, the detection of mitophagy-related proteins demonstrated that GNA significantly enhanced the expression of mitophagy-related proteins in a dose-dependent manner, including OPTN, PINK1, and Parkin1 (Fig. 2E). Collectively, these findings suggested that GNA could promote oxidative stress by breaking the balance of mitochondrial dynamics, and promoting mitochondrial autophagy in McKinley cells.

The apoptotic rate in McKinley cells was significantly enhanced in a dose-dependent manner upon exposure to GNA (Fig. 3A). Further analysis of mitochondrial apoptosis-related genes revealed that, compared to the CON group, the expression of the anti-apoptotic gene BCL2 was significantly reduced in the GNA group. Additionally, there was an increase in the expression levels of pro-apoptotic genes PARP1, BAX, CASP3, and CASP9 with increasing doses of GNA (Fig. 3B). Similarly, a significant increase in the protein expression levels of cleaved PARP1, cleaved Caspase-3, and cleaved Caspase-9 was observed in GNA-treated samples (Fig. 3C). These findings indicate that GNA effectively promotes mitochondrial-related apoptosis in McKinley cells.

GNA enhanced autophagic flux in McKinley cells: The cells observed under the transmission electron microscope revealed that the GNA-M group exhibited numerous vacuoles present in both the cytoplasm and nucleus. The double membrane and mitochondria cristae were not distinctly visible, leading to fragmented mitochondria. Furthermore, there was a substantial increase in autophagosomes in the cytoplasm, where undigested substrates could be observed inside vesicles. Higher electron density secondary lysosomes and lysosomal residues were also evident (Fig. 4A). The AO staining results demonstrated a pronounced increase in the number
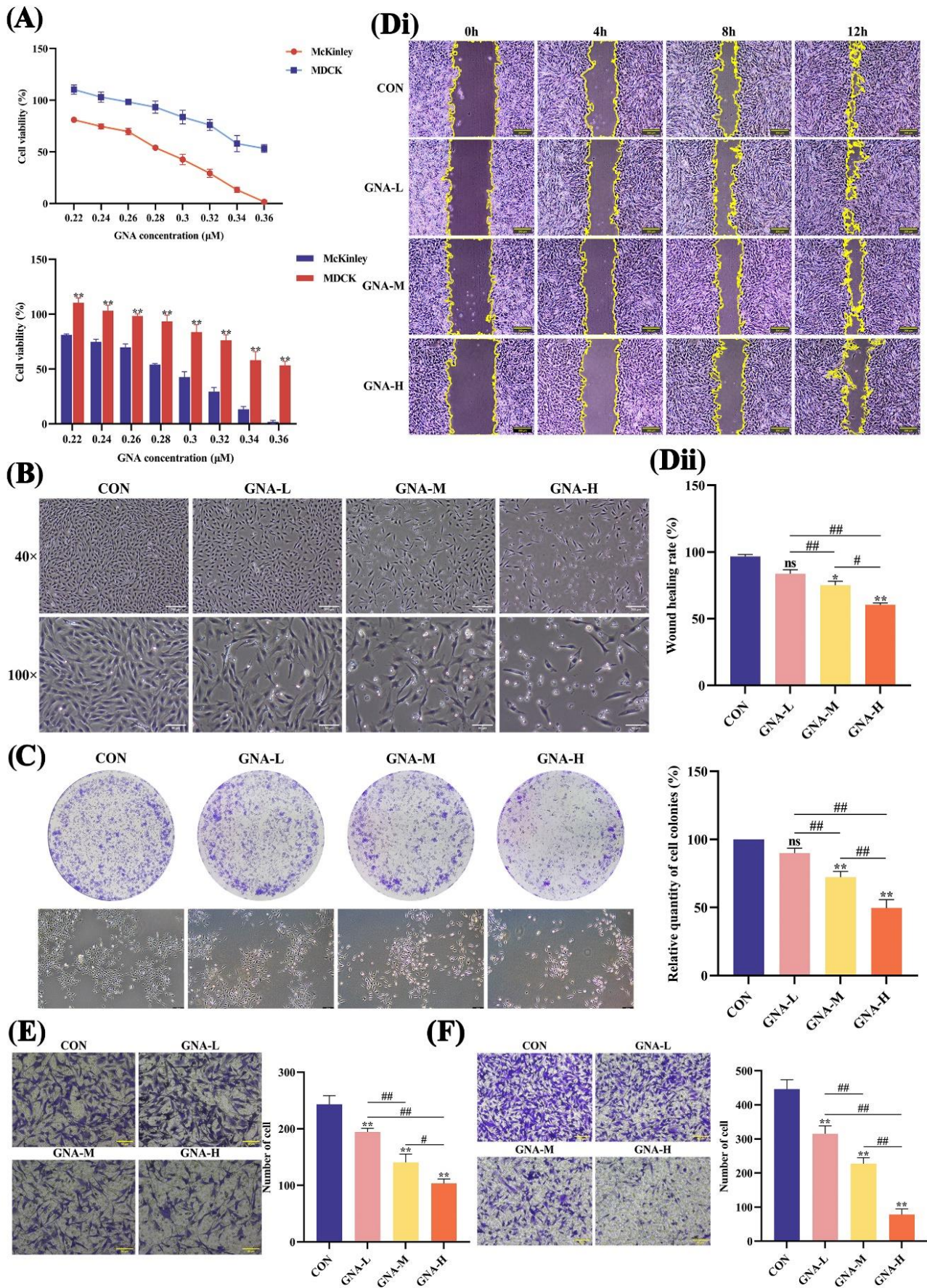
Fig. 1: Effects of GNA on proliferation, migration and invasion of McKinley cells. (A) McKinley cells and MDCK viability were measured with CCK-8 under treating with different concentrations of GNA. (B) Observation of 40× and 100× cell morphology. 40 × scale, 200 μm; 100× scale, 80 μm. (C) Representative photos of cell cloning experiments. Scale, 200 μm. (D) Representative photos and quantization results of cell scratches. Scale, 200 μm. (E-F) Representative photos of Transwell migration and invasion. Scale, 80 μm. Data are expressed as mean ± SD. *P<0.05, **P<0.01, nsP>0.05 versus CON group. #P<0.05, ##P<0.01 indicates a comparison between the two groups.
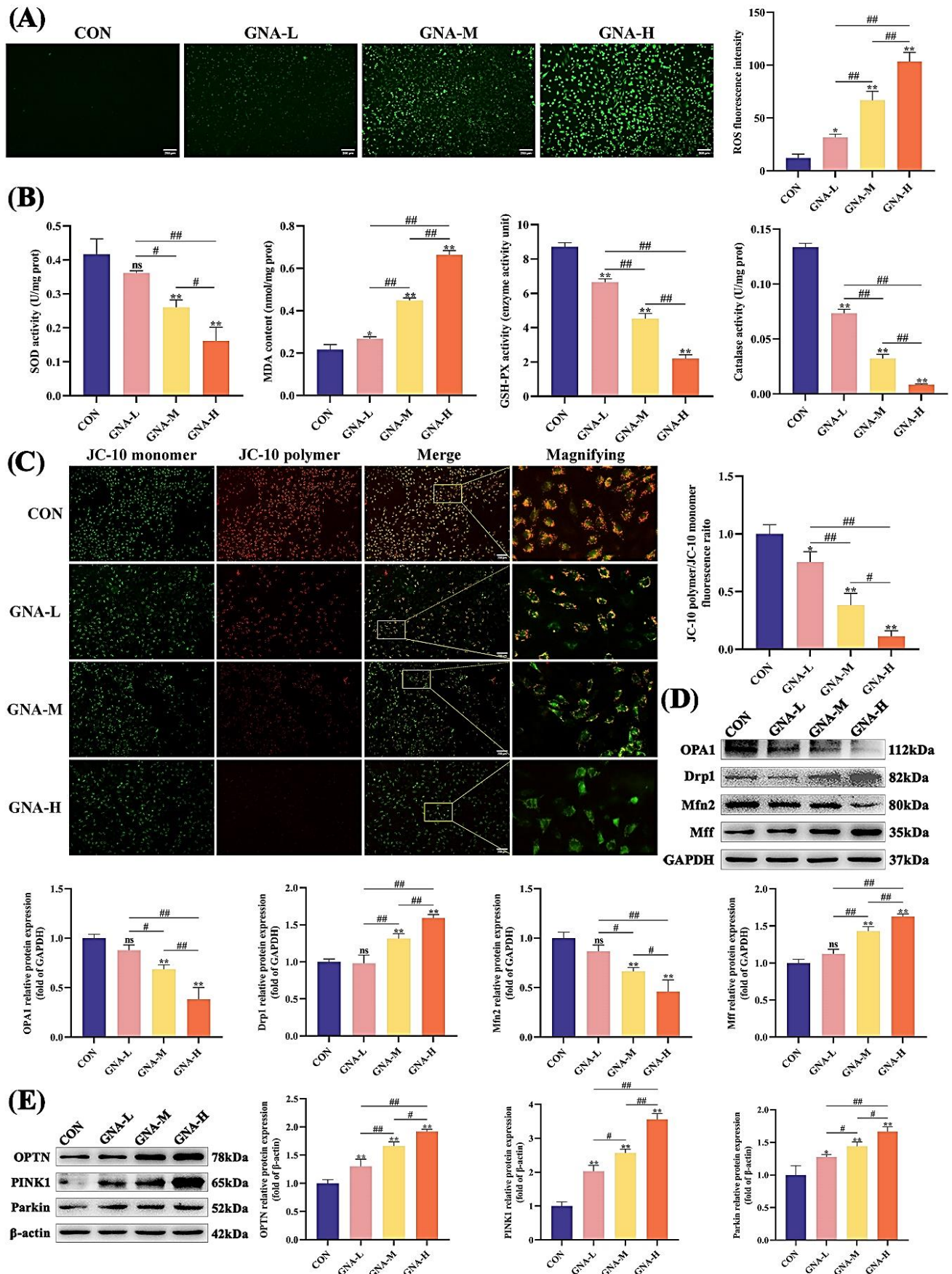
Fig. 2: GNA increased oxidative stress and mitochondrial autophagy in McKinley cells. (A) The degree of intracellular ROS accumulation. Scale, 200 μm. (B) The activity of CAT, SOD and GSH-PX enzymes and content of intracellular MDA in cells. (C) Representative picture of mitochondrial membrane potential detection. Scale, 200 μm. (D-E) Mitochondrial dynamics and mitochondrial autophagy-related protein were detected by Western Blot. Data are expressed as mean ± SD. *P<0.05, **P<0.01, ^{ns}P>0.05 versus CON group. $^{#}$P<0.05, $^{##}$P<0.01 indicates a comparison between the two groups.
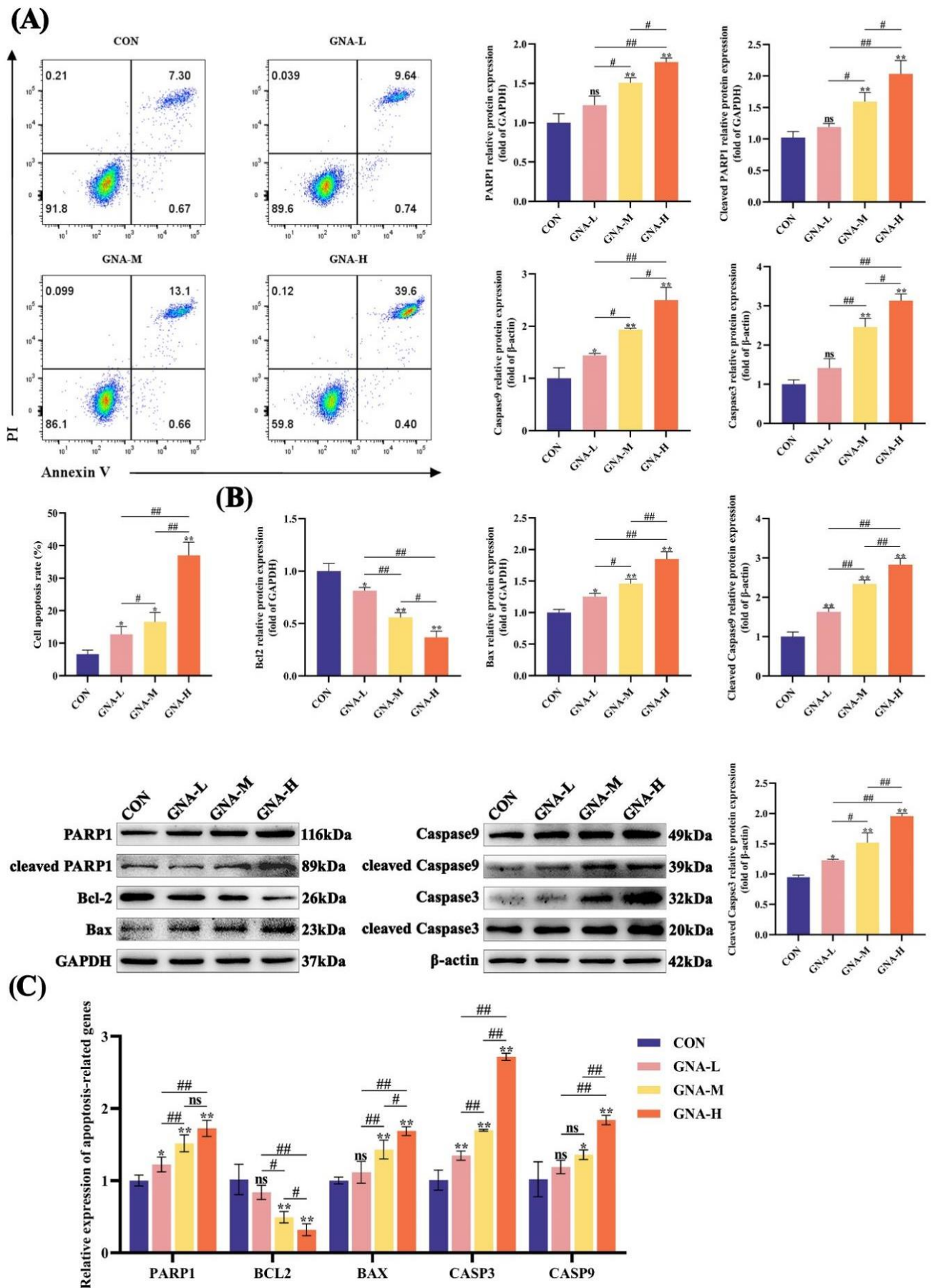
(A)

(B)

(C)

Fig. 3: GNA promoted apoptosis in McKinley cells. (A) The apoptosis of McKinley cells was analyzed by flow cytometry. (B) Apoptosis-related genes mRNA were detected by RT-PCR. (C) Apoptosis-related proteins in the mitochondrial pathway were detected by Western Blot. Data are expressed as mean ± SD. *P<0.05, **P<0.01, nsP>0.05 versus CON group. #P<0.05, ##P<0.01 indicates a comparison between the two groups.

of red fluorescent spots and the intensity of fluorescence signals in a dose-dependent manner within the GNA treatment group compared to the CON group (Fig. 4B).

The expression of autophagy marker protein LC3 was upregulated following GNA treatment as observed by immunofluorescence staining (Fig. 5A). The expression of LC3II was elevated with an increasing dose of GNA. At the same time, there was a notable increase in the conversion of LC3I to LC3II. Autophagy protein ULK1, ATG5-Atg12 complexes, and Beclin1 expression levels were significantly enhanced under GNA. Additionally, the expression of the autophagy substrate p62 was decreased in response to GNA (Fig. 5B). The negative regulatory pathway involving PI3K/AKT/mTOR, which operates upstream of autophagy, was characterized, revealing that the expression levels of p-mTOR, p-PI3K, and p-AKT

decreased in a dose-dependent manner with GNA treatment (Fig. 5C). Additionally, autophagy-related genes mRNA under GNA demonstrated an increase in the expression levels of ATG5, ATG7, ATG12, BECN1, and MAP1LC3B (Fig. 5D). The above results indicate that GNA enhances the autophagic flux of McKinley cells.

GNA enhanced autophagy flow in McKinley cells: To more accurately monitor alterations in autophagic flux, McKinley cells were transiently transfected with pCMV-mCherry-GFP-LC3B, and the depicted results are presented in Fig. 6A. Under the influence of GNA, there is a dose-dependent increase in intracellular mCherry red fluorescence. Concurrently, the GFP green fluorescence was significantly attenuated, indicating that GNA could modulate the processing of LC3 expression. Its
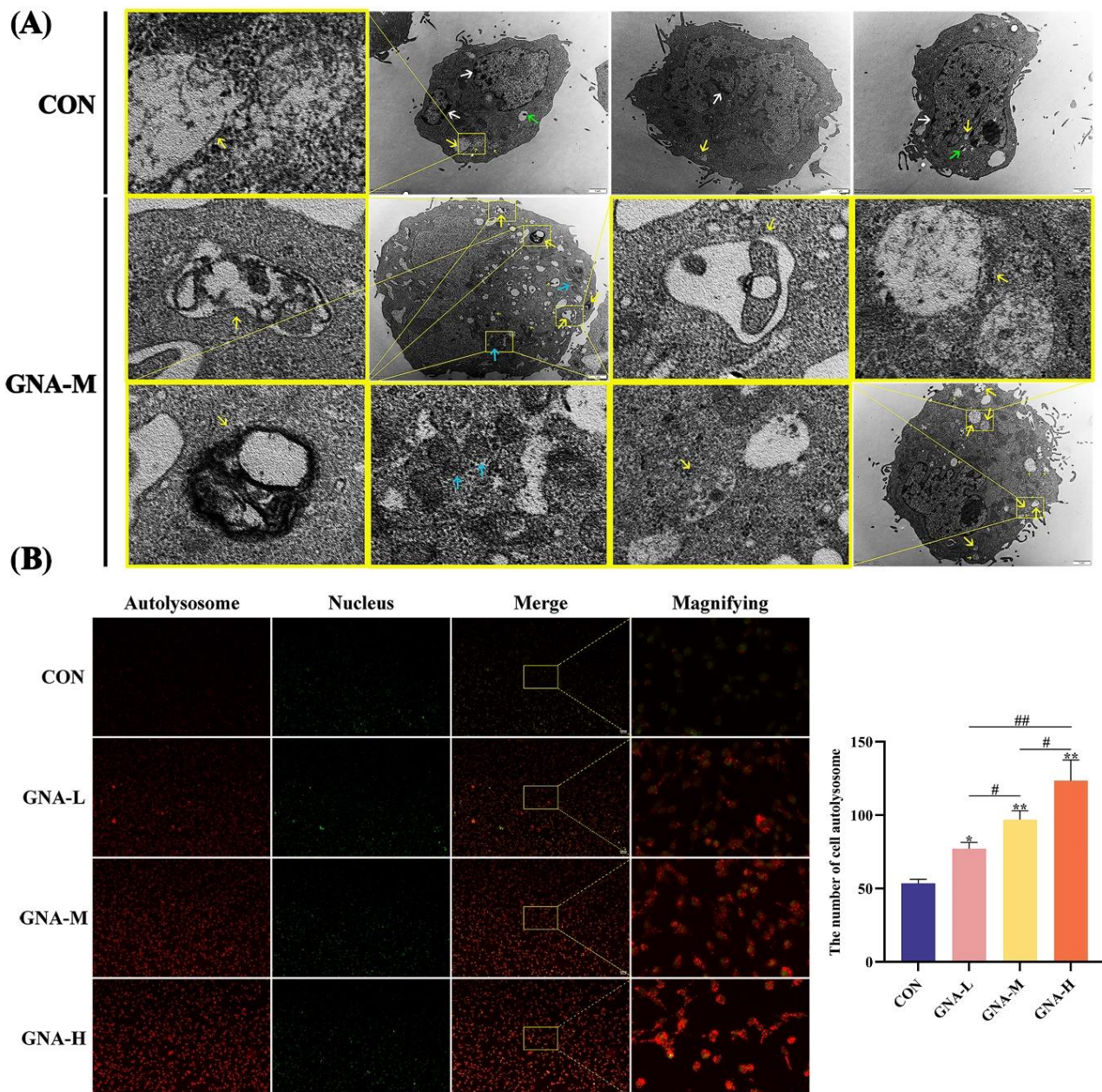

Fig. 4: GNA enhanced autophagic flux in McKinley cells. (A) A representative picture of McKinley cells' ultrastructure. Yellow arrows indicate autophagy vesicles; Green arrows indicate lysosomes in autophagy; white arrow indicates heterochromatin clumped in the inner part of the nuclear envelope; Blue arrows indicate mitochondria. Scale, 1 μm (B) AO staining was used to observe intracellular autophagy vacuoles. Scale, 200 μm. Data are expressed as mean ± SD. *P<0.05, **P<0.01, nsP>0.05 versus CON group. #P<0.05, ##P<0.01 indicates a comparison between the two groups.
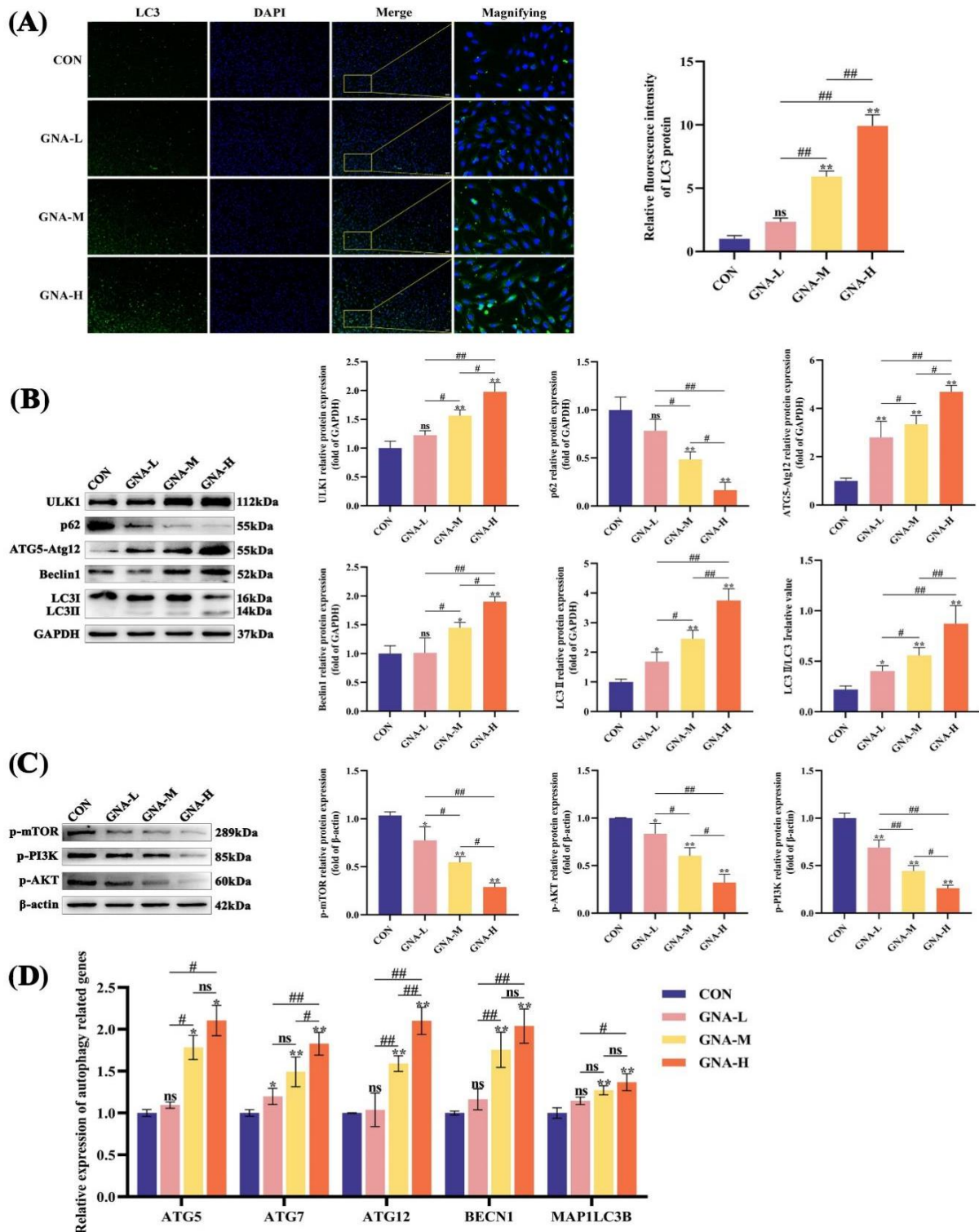
Fig. 5: GNA increased autophagy in McKinley cells. (A) The expression level of LC3 in cells was detected. Scale, 200 μm. (B) Autophagy-related proteins were detected by Western Blot (C) PI3K/AKT/mTOR pathway-related proteins were detected by Western Blot. (D) Autophagy-related genes mRNA were detected by RT-PCR. Data are expressed as mean ± SD. *P<0.05, **P<0.01, ns p >0.05 versus CON group. #P<0.05, ##P<0.01 indicates a comparison between the two groups.

accumulation on the autophagosomal membrane, and the subsequent alteration in autophagic circulation, with a higher level of autophagic flux was observed in a dose-dependent manner. CQ, acting as a late-stage autophagy inhibitor, facilitated further exploration of autophagic flux dynamics. Plasmid transfection revealed a significant enhancement of mCherry and GFP fluorescence accumulation in the GNA-M+CQ group compared to the GNA-M and the CQ group individually (Fig. 6E). Western

Blot analysis demonstrated a marked increase in LC3II levels in the GNA-M+CQ group, revealing a significant contrast when compared to the GNA-M group (Fig. 6B). Upon transmission electron microscopy, a marked increase in the number of autophagosomes was observed in the GNA-M+CQ group compared to the GNA-M group. Additionally, the cells exhibited extensive filling with numerous giant and undigested autophagosomes (Fig. 6C). The results from AO staining further collaborated that GNA
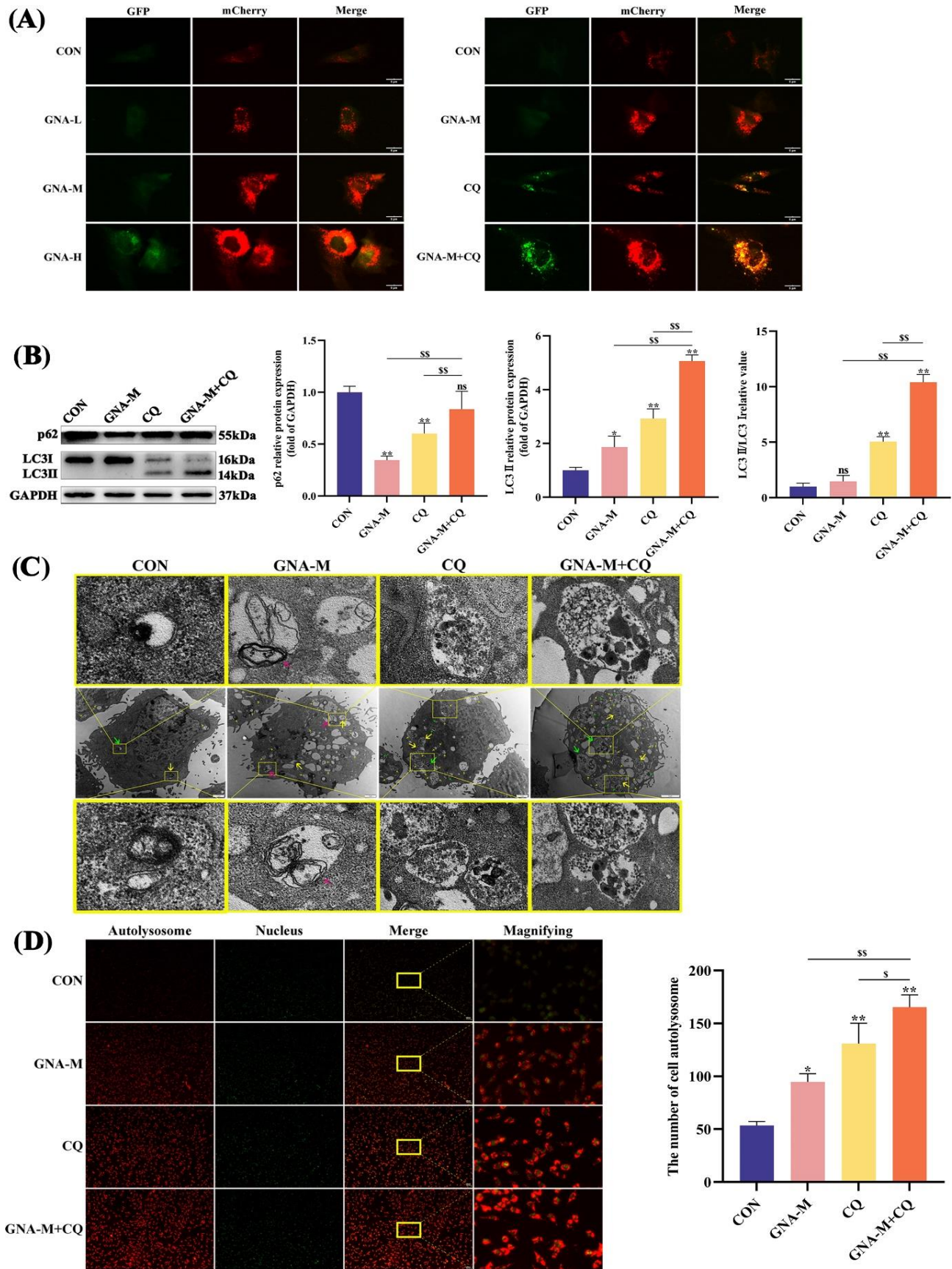
Fig. 6: GNA combined with CQ promotes autophagy flow normally in McKinley cells. (A) GFP-mCherry double fluorescently labeled LC3 plasmid transfected to track autophagy flow level. Scale, 5 μm. (B)Autophagy-related proteins with CQ intervention were detected by Western Blot. (C) Ultrastructure observation of autophagosomes with CQ intervention. Yellow arrows indicate autophagy vesicles; Green arrows indicate lysosomes in autophagy; white arrow indicates heterochromatin clumped in the inner part of the nuclear envelope; Pink arrows indicate undigested mitochondria in autophagy vacuoles. Scale, 1 μm (D)The autophagy vacuoles were observed by AO staining. Scale, 200 μm. (E)Tracking autophagy flow with CQ intervention. Scale, 5 μm. Data are expressed as mean ± SD. *P<0.05, **P<0.01, ^{ns}P>0.05 versus CON group. $^\&$P<0.05, $^{\&\&}$P<0.01 indicates a comparison between the two groups.

significantly enhanced autophagic flux in McKinley cells (Fig. 6D). Collectively, these findings indicate that autophagic flow was unimpeded under GNA, with a significant enhancement in the level of autophagic flux in McKinley cells.

3-MA could reverse the rise in autophagy in McKinley cells caused by GNA: To investigate the role of autophagy in the inhibition of McKinley cells by GNA, 3-MA was used to inhibit early autophagy in the present study. Our findings indicated that a concentration of

350µM 3-MA was innocuous to McKinley, as evidenced by both CCK-8 assays (Fig. 7A). The results from cell immunofluorescence (Fig. 7B), AO staining (Fig. 7C), and the expression of autophagy-related proteins (Fig. 7D) demonstrated that 350µM 3-MA significantly inhibited the level of autophagy in McKinley cells. Compared with the GNA group, the 3-MA+GNA group further decreased the autophagy level in McKinley cells. Additionally, 3-MA was able to reverse the increase in autolysosomes and the expression of autophagy-related proteins induced by GNA.
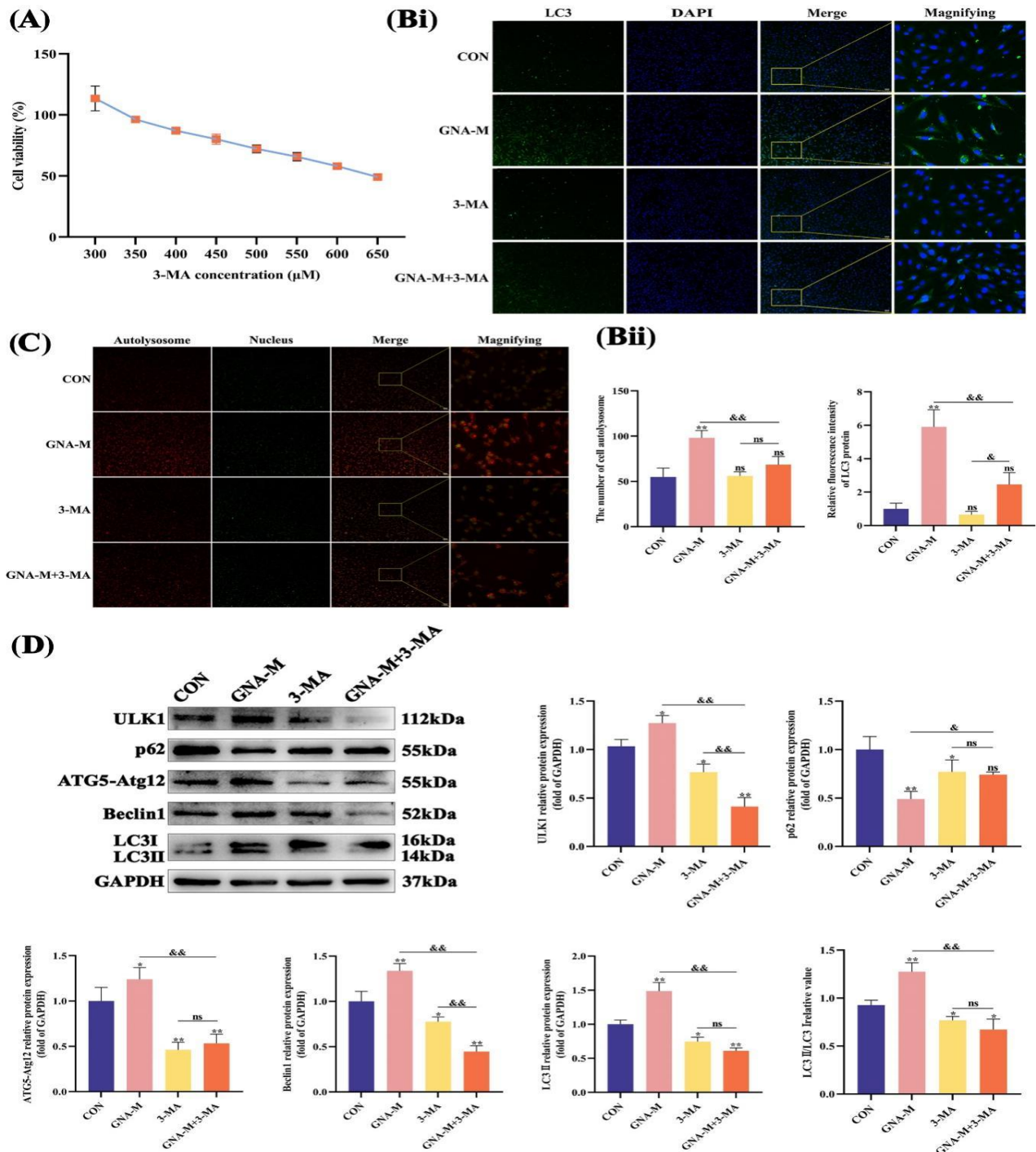
Fig. 7: 3-MA reversed the increase in autophagy caused by GNA in McKinley cells. (A)The effect of 3-MA on cell viability was detected by CCK-8 assay. (B) LC3 expression was detected by immunofluorescence assay after the combination of GNA and 3-MA. Scale, 200 µm. (C) Intracellular autophagy vacuoles were detected by AO staining after 3-MA intervention. Scale, 200 µm. (D) Apoptosis-related proteins in mitochondria were detected by Western Blot. Data are expressed as mean ± SD. $^*P<0.05$, $^{**}P<0.01$, $^{ns}P>0.05$ versus CON group. $^{\&}P<0.05$, $^{\&\&}P<0.01$ indicates a comparison between the two groups.

3-MA could partially rescue the inhibition of proliferation, migration, and invasion in McKinley cells caused by GNA: 3-MA effectively mitigated the cytotoxic effects induced by GNA across various concentrations (Fig. 8A). Furthermore, cellular morphology examination (Fig. 8B), cell clonogenic assay (Fig. 8C), cell wound healing assay (Fig. 8D), and

Transwell migration and invasion assay (Fig. 8E-F), revealed that 3-MA can counteract the detrimental effects of GNA on cell proliferation, migration, and invasion capabilities. These results indicate that inhibition of autophagy can partially rescue the inhibition of proliferation, migration, and invasion caused by GNA in McKinley cells.
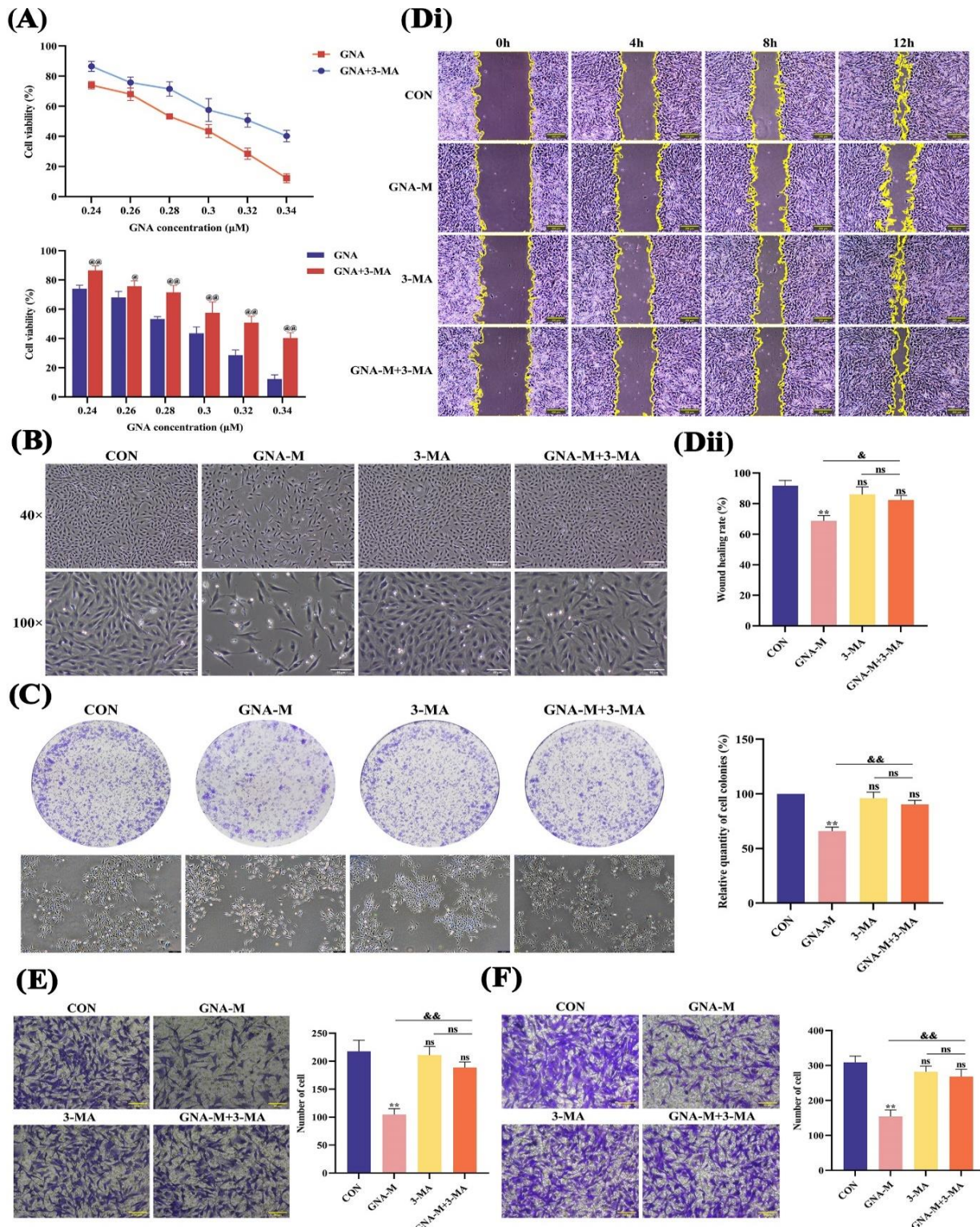

Fig. 8: 3-MA rescued the inhibition of proliferation, migration, and invasion by GNA in McKinley cells. (A) The effect of 3-MA and GNA on cell viability was detected by the CCK-8 method. *P<0.05, **P<0.01 versus CON group. (B) The morphology of 40× and 100× cells was observed by an inverted microscope. 40 × scale, 200 μm. 100 × scale, 80 μm. (C) Representative picture of clonal formation test. (D) Representative photos and quantization results of cell scratches. Scale, 200 μm. (E-F) Representative photos of Transwell migration and invasion. Scale, 80 μm. Data are expressed as mean ± SD. @P<0.05, @@P<0.01 versus GNA group. *P<0.05, **P<0.01, nsP>0.05 versus CON group. &P<0.05, &&P<0.01 indicates a comparison between the two groups.

3-MA could partially rescue GNA-induced oxidative stress and apoptosis levels in McKinley cells: The findings indicate that, in comparison to the GNA-M group, the GNA-M+3-MA group exhibited a marked reduction in ROS levels (Fig. 9A) and MDA levels (Fig. 9B), concomitant with a significant increase in the activities of SOD, GSH-PX, and CAT (Fig. 9B). Data obtained from JC-10 staining revealed a substantial augmentation in mitochondrial membrane potential within the GNA-M+3-MA group, in comparison to the GNA-M group, with no significant difference observed when compared with the CON group (Fig. 9C). Detections of mitochondrial dynamics-related proteins (Fig. 9D) and mitochondrial

autophagy-related proteins (Fig. 9E) indicate that combination treatment with 3-MA and GNA promoted mitochondria fusion, while mitophagy and fission processes were diminished. Flow cytometry analysis revealed that 3-MA mitigated the pro-apoptotic effects of GNA in McKinley cells (Fig. 10A). Furthermore, the analysis of mitochondrial apoptosis-related proteins (Fig. 10B) and mRNA (Fig. 10C) revealed that 3-MA can counteract the impact of GNA on apoptosis-related markers. The results of the above tests indicate that 3-MA can reverse oxidative stress levels and apoptosis caused by GNA in McKinley cells.
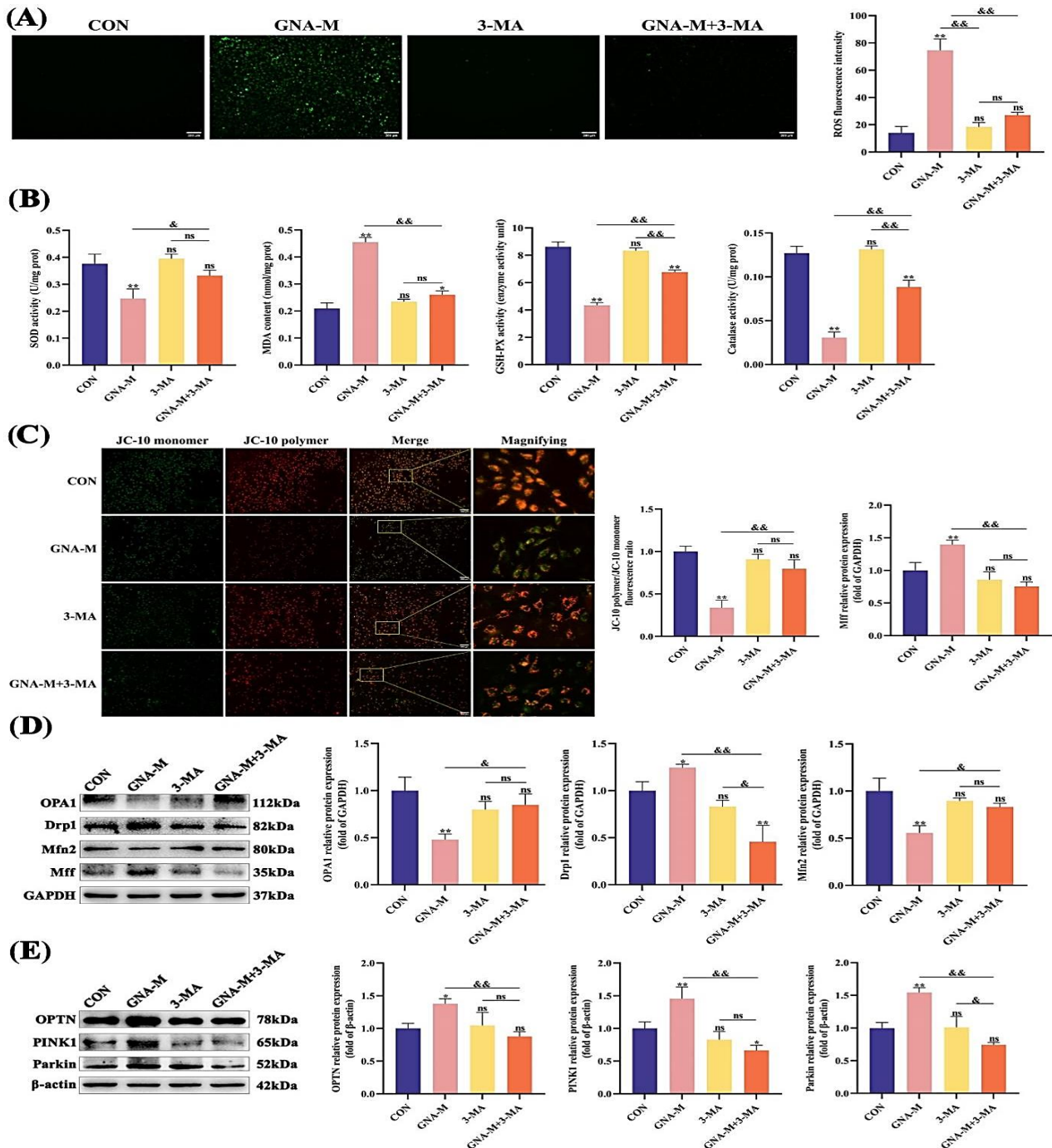

Fig. 9: 3-MA rescued oxidative stress and mitochondrial autophagy by GNA in McKinley cells. (A) The degree of intracellular ROS accumulation. Scale,200 μm. (B)The activity of CAT, SOD and GSH-PX enzymes and content of intracellular MDA in cells. (C)Representative picture of mitochondrial membrane potential detection. Scale,200 μm. (D、E) Mitochondrial dynamics and mitochondrial autophagy-related protein expression were detected by Western Blot. Data are expressed as mean ± SD. *P<0.05, **P<0.01, nsP>0.05 versus CON group. &P<0.05, &&P<0.01 indicates a comparison between the two groups.
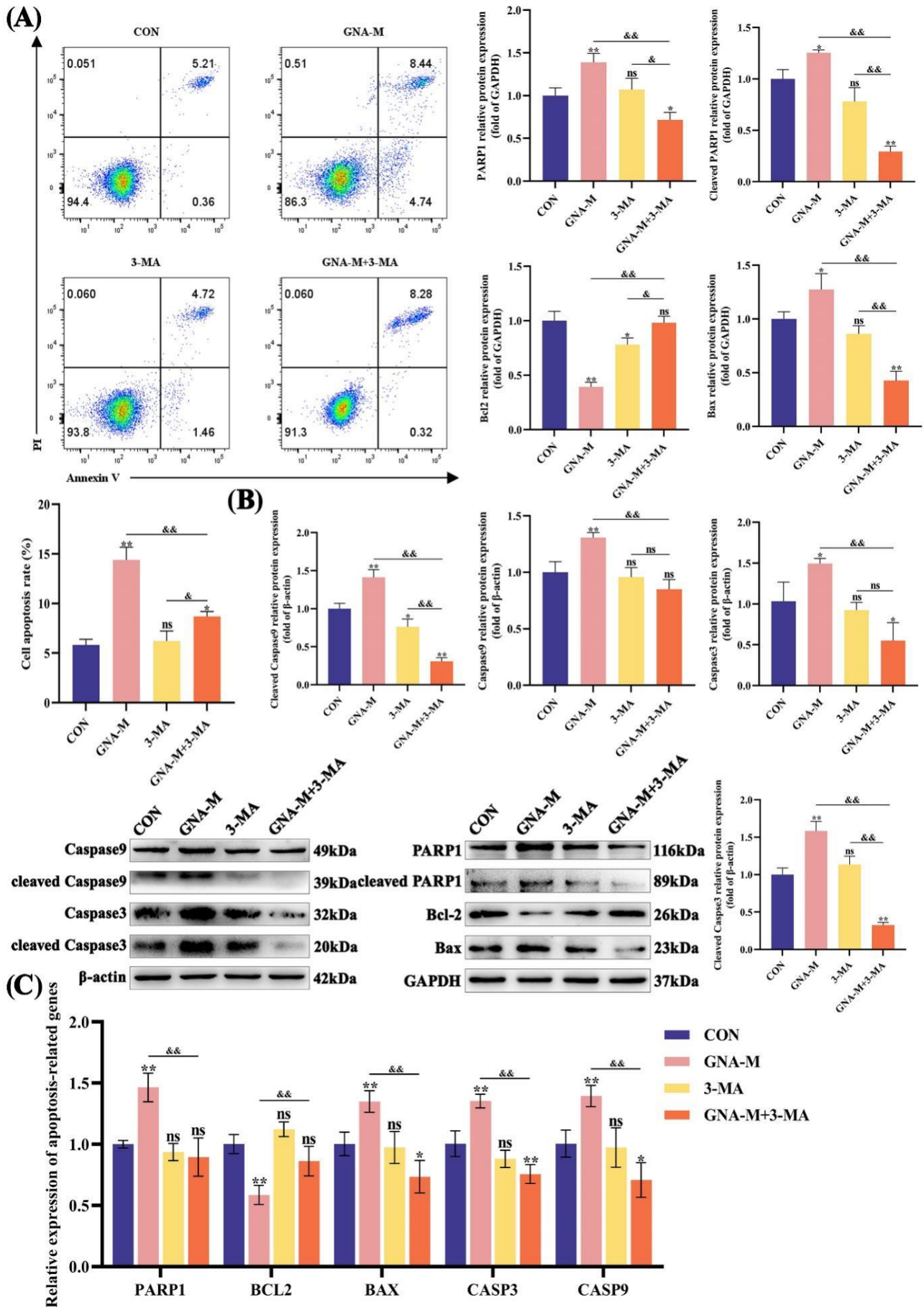
Fig. 10: 3-MA rescued apoptosis by GNA in McKinley cells. (A) Cell apoptosis rate was determined by flow cytometry (B) Apoptosis-related protein was detected by Western Blot. (C) Apoptosis-related genes mRNA in the mitochondrial pathway was detected by RT-PCR. Data are expressed as mean ± SD. $^*P<0.05$, $^{**}P<0.01$, $^{ns}P>0.05$ versus CON group. $^&P<0.05$, $^{&&}P<0.01$ indicates a comparison between the two groups.

DISCUSSION

Canine OS accounts for approximately 80% of malignant bone tumors in dogs *(Szewczyk et al.,* 2015), seriously harming the life, health, and quality of life of the affected dogs. GNA has been reported to possess anti-tumor pharmacological properties. However, its potential to inhibit canine osteosarcoma remains unclear. In this study, we examined the inhibitory effects of GNA on canine OS in McKinley cells with GNA and explored the role of autophagy in mediating GNA's effects against this condition through 3-MA. Our findings suggest that GNA could demonstrate anti-canine OS effects via autophagy.

In this study, the cytotoxicity of GNA towards McKinley cells and MDCK cells was evaluated utilizing the CCK-8 assay. The IC$_{50}$ of GNA was determined to be 0.28μM in McKinely cells, while the MDCK cells survival rate was 93.3%, and 7μM in human lung cancer A549 cells at the same cell viability (Yu *et al.*, 2012). It indicated that McKinley cells were more sensitive to GNA. Besides, the effective limitation of the motility of OS is widely recognized as a critical indicator of the treatment effect on OS metastasis (Szewczyk *et al.*, 2015). The Transwell assay and the wound healing assay can reflect the motility of cells. GNA has been shown to significantly interfere with the mobility of McKinley cells. This is consistent with the results of Zhou *et al.* (2020) who employed 1.5μM GNA to alter the tumor microenvironment (TME) through the NF-κB pathway, thereby mediating the activity transformation of various cell adhesion factors to inhibit the metastasis of bladder cancer BIU-87, T24, and J82 cells, indicating that GNA may have the potential to suppress OS metastasis.

GNA has been shown to inhibit various tumors, such as nasopharyngeal carcinoma (Yan *et al.*, 2011), by enhancing oxidative stress. Consistent with the previous, GNA also increased the oxidative stress level in McKinley cells. Mitochondria is a major source of ROS production. Our research findings indicate that exposure of McKinley cells to GNA results in a decrease in MMP and an increased tendency for mitochondrial fission, ultimately leading to mitochondrial dysfunction. In addition, this study observed a notable increase in apoptosis rate and upregulation of pro-apoptotic factors detected in the present study, supporting that GNA promoted apoptosis in McKinley cells via the mitochondrial pathway-mediated apoptosis. These results are consistent with the findings of Liu *et al.* (2021) who reported that atezolizumab exerted tumor suppression by extensively regulating mitochondria in OS cells, causing mitochondria-related apoptosis (Buondonno *et al.*, 2016; Liu *et al.*, 2021; Yen *et al.*, 2019).

Autophagy transports functionally impaired biological macromolecules, aging, or damaged organelles to lysosomes for degradation and reutilization via various pathways. The quantification of autophagosomes serves as an indicator of the autophagic activity within cells. In the present study, GNA significantly enhanced the number of autophagosomes, with analogous effects noted in A549 (Wang *et al.*, 2014). mTOR is the key regulator in the autophagy signaling pathway, could suppress the activity of the autophagy initiator protein ULK1 (Kim *et al.*, 2011). This study indicated that the PI3K/AKT/mTOR signaling pathway was inhibited by GNA, leading to a diminished inhibitory effect of mTOR on autophagy, thereby promoting autophagic processes. Comparable results were reported in the study conducted by Yu X J, where a time-dependent decrease in the expression levels of p-Akt and p-mTOR proteins was observed in H1975 and H460 cells treated with GNA(Yu *et al.*, 2012). Moreover, autophagy represents a crucial process occurring at the protein level. This study further investigated the impact of GNA on the expression of autophagy-related proteins, which exhibited a dose-dependent increase in response to GNA, while the expression of p62 decreased in a dose-dependent manner. Additionally, previous research has indicated that mitochondrial fission can trigger mitophagy to eliminate damaged mitochondria, a phenomenon corroborated by our results. The mentioned results suggest that GNA effectively promotes autophagy in McKinley cells. Nevertheless, autophagy is a dynamic process; an increase in the number of autophagosomes does not necessarily correlate with a proportional rise in autophagic flux. We integrated GNA with CQ and observed that GNA did not impede the late stages of autophagy in McKinley cells, and the autophagy levels exhibited an upward trajectory, differing from other tumor cell types. In A549 and BEL-7402/ADM, GNA has been shown to activate autophagy while concurrently inhibiting its late stages, leading to a blockade of autophagic flux and preventing the degradation of autophagic vesicle contents (Hillers *et al.*, 2005; Wang *et al.*, 2014). Currently, it is hypothesized that this differential effect of GNA may stem from its varying impacts on lysosomal function. Collectively, these findings suggest that GNA inhibits the PI3K/AKT/mTOR signaling pathway, while activating autophagy in McKinley cells without disrupting the formation and degradation of autolysosomes and enhancing the overall autophagic flux within cells.

A notable elevation in autophagy levels within McKinley cells following GNA treatment was also noticed. Considering the duality of the role of autophagy in cancer, we aimed to utilize 3-MA to investigate the precise function of autophagy under GNA in McKinley cells. 3-MA was employed to suppress autophagy, and the inhibition effectively counteracted the effects of GNA on the proliferation, migration, and invasion of McKinley cells. These findings indicate that autophagy promoted by GNA is excessive and does not promote tumor cell growth. Autophagy interacts with various cellular processes to regulate tumor development and progression. In the presence of 3-MA, the effects of GNA on oxidative stress, mitochondrial function, and apoptosis-related indexes in McKinley cells were attenuated, further suggesting that GNA could promote excessive autophagy. Similar findings can also be confirmed in Mei W's research, which indicates that GNA can induce the accumulation of autophagic vesicles in A549 and HeLa cells by significantly upregulating Beclin1 expression, consequently increasing the apoptosis rate (Wang *et al.*, 2014). It is important to note that the relationship between autophagy, oxidative stress, and apoptosis is not static. As shown by Wear D, 3-MA can enhance both apoptosis and oxidative stress levels in neuroblastoma cells treated with cisplatin and temozolomide (Wear *et al.*, 2023). Taken together, the present study confirmed that GNA promoted apoptosis and oxidative stress by over-activating autophagy in McKinley cells.

GNA-induced cell death exhibits similarities to autophagy-dependent cell death (ADCD), with excessive autophagy being the main contributor to the demise of the cell (Ritter and Bielack, 2010). In the A549 lung cancer ADCD model induced by resveratrol, the number of autolysosomes continues to increase progressively with the duration of cell death (Dasari *et al.*, 2017). In the present study, under the influence of GNA, there was a significant enhancement of autophagy during cell death, alongside apoptosis occurring. Although not classified as ADCD, it offered valuable insights into the underlying mechanisms. Furthermore, although autophagy may facilitate the progression of advanced tumors, it has the potential to eliminate tumor cells via ADCD when therapeutic interventions are applied. It is worth noting that some studies have found that gambogic acid (GA) can bind to Bcl-2 by competitively binding with BH3 peptides, thereby releasing pro-apoptotic proteins *(Zhai et al.*, 2008). The interaction between Beclin1 and Bcl-2 represents an important mechanism to link autophagy and apoptosis. Beclin1 interacts with Bcl-2 through the BH3 domain, thereby GA may promote autophagy by competitively binding to Bcl-2 to separate Beclin1. Due to the structural similarity between GNA and GA, it is plausible that GNA may also have a similar role. In this investigation, GNA treatment resulted in increasing the expression of Beclin1, decreasing the expression of Bcl-2 and the proportion of heterodimers. The free Beclin1 activated autophagy, while the increased expression of Bax promoted the level of apoptosis. Therefore, GNA may exert its anti-tumor effects through mechanisms akin to ADCD, thereby providing theoretical support for the application of GNA in tumor cells lacking apoptotic mechanisms. A diverse array of natural compounds can also fulfill this function. The BH3 domain mimics Gosselin can competitively interact with Bcl-2 through Beclin1, thereby liberating Beclin1 to trigger autophagy and inhibiting Bcl-2 to facilitate cellular apoptosis (Gola *et al.*, 2021; Rosenblum *et al.*, 2015).

Conclusions: GNA provokes oxidative stress, disrupts mitochondrial function, and triggers mitochondrial apoptosis through the upregulation of McKinley cells autophagy. Furthermore, this study did not evaluate the *in vivo* anti-tumor effects of GNA, the comparative effects of GNA against chemotherapeutic agents in McKinley cells, or the precise mechanisms linking autophagy and apoptosis. Subsequent trials are therefore needed to completely explore the underlying mechanism in this regard.

Authors contribution: Xiaoyu Hou and Tianyuan Yang conceived and designed the study. Siyao Li, Xiaoyu Hou, Huijie Kang, Qingdian Hou, and Yuntong Zhang executed the experiment and analyzed the cell samples. Siyao Li, Yuan Zhao, and Xiaoyu Hou analyzed and interpreted the data. Shuai Zhang, Weiqian Wang, Meimei Wang, Guangmin Zhang, and Junping Sun collected research background data. Siyao Li, Yuan Zhao, and Xiaoyu Hou wrote manuscripts. Honggang Fan and Jichen Sha critically revised the manuscript for important intellectual content and approved the final version.

Declaration of competing interests: No conflict of interest exists in submitting this manuscript.

REFERENCES

Aqbi HF, Tyutyunyk-Massey L, Keim RC, *et al.*, 2018. Autophagy-deficient breast cancer shows early tumor recurrence and escape from dormancy. Oncotarget 9:22113-22122.

Buondonno I, Gazzano E, Jean SR, *et al.*, 2016. Mitochondria-Targeted Doxorubicin: A New Therapeutic Strategy against Doxorubicin-Resistant Osteosarcoma. Mol Cancer Ther 15:2640-2652.

Chen R, Zhang H, Chen B, *et al.*, 2017. Gambogenic Acid Enhances Chemosensitivity of Multiple Myeloma to Bortezomib through p53/ROS/p38 MAPK Apoptotic Pathway. Blood 130:5394.

Dasari SK, Bialik S, Levin-Zaidman S, *et al.*, 2017. Signalome-wide RNAi screen identifies GBA1 as a positive mediator of autophagic cell death. Cell Death Differ 24:1288-1302.

Fujii S, Mitsunaga S, Yamazaki M, *et al.*, 2008. Autophagy is activated in pancreatic cancer cells and correlates with poor patient outcome. Cancer Sci 99:1813-19.

Gola C, Giannuzzi D, Rinaldi A *et al.*, 2021. Genomic and Transcriptomic Characterization of Canine Osteosarcoma Cell Lines: A Valuable Resource in Translational Medicine. Front Vet Sci 8:666838.

Hillers KR, Dernell WS, Lafferty MH, *et al.*, 2005. Incidence and prognostic importance of lymph node metastases in dogs with appendicular osteosarcoma: 228 cases (1986-2003). J Am Vet Med Assoc 226:1364-67.

Huang KM, Chen YY, Zhang R, *et al.*, 2018. Honokiol induces apoptosis and autophagy via the ROS/ERK1/2 signaling pathway in human osteosarcoma cells in vitro and in vivo. Cell Death Dis 9(2):157.

Huang Q, Guo K, Ren Y, *et al.*, 2024. Design, synthesis, and biological evaluation of gambogenic acid derivatives: Unraveling their anti-cancer effects by inducing pyroptosis. Bioorg Chem 145:107182.

Kim J, Kundu M, Viollet B, *et al.*, 2011. AMPK and mTOR regulate autophagy through direct phosphorylation of Ulk1. Nat Cell Biol 13:132-41.

Liu Z, Wang H, Hu C, *et al.*, 2021. Targeting autophagy enhances atezolizumab-induced mitochondria-related apoptosis in osteosarcoma. Cell Death Dis 12(2):164.

Liu Z, Wang X, Li J, *et al.*, 2023. Gambogenic acid induces cell death in human osteosarcoma through altering iron metabolism, disturbing the redox balance, and activating the P53 signaling pathway. Chem Biol Interact 382:110602.

Long XH, Zhou YF, Lan M, *et al.*, 2019. Valosin-containing protein promotes metastasis of osteosarcoma through autophagy induction and anoikis inhibition via the ERK/NF-κβ/beclin-1 signaling pathway. Oncol Lett 18:3823-29.

Pan ZF, Xu T, Bao LS, *et al.*, 2022. CREB3L1 promotes tumor growth and metastasis of anaplastic thyroid carcinoma by remodeling the tumor microenvironment. Mol Cancer 21(1):190.

Parlayan C, Sahin Y, Altan Z, *et al.*, 2021. ARID3A regulates autophagy related gene BECN1 expression and inhibits proliferation of osteosarcoma cells. Biochem Biophys Res Commun 585:89-95.

Poon AC, Matsuyama A, Mutsaers AJ, 2020. Recent and current clinical trials in canine appendicular osteosarcoma. Can Vet J 61:301-08.

Ritter J, Bielack SS, 2010. Osteosarcoma. Ann Oncol 21:320-25.

Rosenblum JM, Wijetunga NA, Fazzari MJ, et al., 2015. Predictive properties of DNA methylation patterns in primary tumor samples for osteosarcoma relapse status. Epigenetics 10:31-39.

Selmic LE, Burton JH, Thamm DH, *et al.*, 2014. Comparison of Carboplatin and Doxorubicin-Based Chemotherapy Protocols in 470 Dogs after Amputation for Treatment of Appendicular Osteosarcoma. J Vet Intern Med 28:554-63.

Szewczyk M, Lechowski R, Zabielska K, 2015. What do we know about canine osteosarcoma treatment? – review. Vet Res Commun 39:61-67.

Tavakolikazerooni H, Tariq M, Yu H, *et al.*, 2025. Melatonin Modulates Necroptosis and Enhances Antioxidant Defense during PGF-Induced Luteal Regression in Heat-Exposed Rats. Pak Vet J 45: 205-15.

Wang M, Chen D, Cheng H, *et al.*, 2014. Gambogenic Acid Kills Lung Cancer Cells through Aberrant Autophagy. Plos One 9(1):e83604.

Wang M, Cheng H, Wu H, *et al.*, 2022. Gambogenic acid antagonizes the expression and effects of long non-coding RNA NEAT1 and triggers autophagy and ferroptosis in melanoma. Biomed Pharmacother 154:113636.

Wear D, Bhagirath E, Balachandar A, *et al.*, 2023. Autophagy Inhibition via Hydroxychloroquine or 3-Methyladenine Enhances Chemotherapy-Induced Apoptosis in Neuro-Blastoma and Glioblastoma. Int J Mol Sci 24(15):12052.

Wei H, Wang C, Croce CM, *et al.*, 2014. p62/SQSTM1 synergizes with autophagy for tumor growth in vivo. Genes Dev 28:1204-16.

Weiss MC, Eulo V, Van Tine BA, 2022. Truly Man's Best Friend: Canine Cancers Drive Drug Repurposing in Osteosarcoma. Clin Cancer Res 28:571-72.

Wu J, Wang D, Zhou J, *et al.*, 2023. Gambogenic acid induces apoptosis and autophagy through ROS-mediated endoplasmic reticulum stress via JNK pathway in prostate cancer cells. Phytother Res 37(1):310-28.

Yan F, Wang M, Chen H, *et al.*, 2011. Gambogenic acid mediated apoptosis through the mitochondrial oxidative stress and inactivation of Akt signaling pathway in human nasopharyngeal carcinoma CNE-1 cells. Eur J Pharmacol 652:23-32.

Yen JH, Huang HS, Chuang CJ, *et al.*, 2019. Activation of dynamin-related protein 1-dependent mitochondria fragmentation and suppression of osteosarcoma by cryptotanshinone. J Exp Clin Cancer Res 38(1):42.

Yu XJ, Han QB, Wen ZS, *et al.*, 2012. Gambogenic acid induces G1 arrest via GSK3β-dependent cyclin D1 degradation and triggers autophagy in lung cancer cells. Cancer Lett 322:185-94.

Zhai D, Jin C, Shiau Cw, *et al.*, 2008. Gambogic acid is an antagonist of antiapoptotic Bcl-2 family proteins. Mol Cancer Ther 7:1639-46.

Zhao Y, Wang CQ, Yang TY, *et al.*, 2022. Chlorogenic Acid Alleviates Chronic Stress-Induced Duodenal Ferroptosis via the Inhibition of the IL-6/JAK2/STAT3 Signaling Pathway in Rats. Agric. Food Chem 70, 4353-61.

Zhou S, Zhao N, Wang J, 2020. Gambogenic acid suppresses bladder cancer cells growth and metastasis by regulating NF-κB signaling. Chem Biol Drug Des 96:1272-79.